Progress in Microbes and Molecular Biology

HH PUBLISHER

Original Research Article

BuShenFang Suppresses Tumor Growth and Induces Apoptosis in Colorectal Cancer Xenografts

Khang Wen Goh[1], Jie Ji[2*], Xian Gu[3], Lokesh Bontha Venkata Subrahmanya[4], Hemant Kumar Singh Yadav[5], Phei Er Kee[2,6], Siew-Keah Lee[7], Ashok Kumar Janakiraman[8], Long Chiau Ming[9], Kai Bin Liew[2*]

Article History

Received: 03 March 2025;

Received in Revised Form: 27 august 2025;

Accepted: 04 September 2025;

Available Online: 18 September 2025

[1]Faculty of Data Science and Information Technology, INTI International University, Persiaran Perdana BBN Putra Nilai, 71800 Nilai, Negeri Sembilan, Malaysia; khangwen.goh@newinti.edu.my (KWG)

[2]Faculty of Pharmacy, University of Cyberjaya. Persiaran Bestari, 63000 Cyberjaya, Selangor, Malaysia

[3]Department of Oncology 5, Longhua Hospital Affiliated to Shanghai University of Traditional Chinese Medicine, 200032 Xuhui District, Shanghai, China; 13761347124@163.com (XG)

[4]Department of Pharmaceutical Chemistry, Faculty of Pharmacy, University of Malaya, 50603, Kuala Lumpur, Malaysia; drlokesh.bontha@um.edu.my (LBVS)

[5]Department of Pharmaceutical Sciences, Indira Gandhi University, Meerpur, Rewari, India; haisunny2@yahoo.co.in (HKSY)

[6]Biorefinery and Bioprocessing Engineering Laboratory, Department of Chemical Engineering and Materials Science, Yuan Ze University, Chungli, Taoyuan 320, Taiwan; pheier.kee@saturn.yzu.edu.tw (PEK)

[7]M. Kandiah Faculty of Medicine and Health Sciences, Universiti Tunku Abdul Rahman, Jalan Sungai Long, Bandar Sungai Long, Kajang 43000, Selangor, Malaysia; leesiewkeah@utar.edu.my (SKL)

[8]Department of Pharmaceutics, Dr. Kalam College of Pharmacy, Periyanayagipuram, Avanan 614623, Thanjavur, Tamil Nadu, India; akpharm@gmail.com (AKJ)

[9]Faculty of Medical and Life Sciences, Sunway University, Sunway City, 47500 Subang Jaya, Selangor, Malaysia; chiaumingl@sunway.edu.my (LCM)

*Corresponding authors: Jie Ji & Kai Bin Liew; Faculty of Pharmacy, University of Cyberjaya. Persiaran Bestari, 63000 Cyberjaya, Selangor, Malaysia; 2112-4733@st.cyberjaya.edu.my (JJ), liewkaibin@cyberjaya.edu.my (KBL)

Abstract: Colorectal cancer (CRC) remains a major global health burden, necessitating alternative therapeutic approaches. Traditional Chinese Medicine (TCM), including BuShenFang (BSF), has demonstrated potential anti-CRC effects, yet its precise

mechanisms remain unclear. While BSF has previously exhibited anti-CRC activity in vitro, its in vivo efficacy and associated molecular mechanisms requires further elucidation. In this study, a subcutaneous xenograft model was established in nude mice, which lack T-cell-mediated immunity and can effectively support the growth of human colorectal cancer cells (HCT116). This model enables a more clinically relevant evaluation of BSF's antitumor effects in vivo. The study aimed to assess the tumor inhibitory effect of BSF and investigate its underlying mechanisms via the Wnt/β-catenin signaling pathway. Mice were allocated into control, low-dose BSF (L-BSF), high-dose BSF (H-BSF), and xStAxVHLL (positive control) groups. Tumor growth was monitored, and analyses including histology, immunohistochemistry, TUNEL assay, immunofluorescence, and Western blotting were performed to examine tumor proliferation, apoptosis, and Wnt pathway regulation. BSF significantly inhibited tumor growth in a dose-dependent manner, reduced KI67 expression, promoted apoptosis, and increased adenomatous polyposis coli (APC) levels. Additionally, BSF downregulated β-catenin, p-GSK-3β/GSK-3β, and Axin1, while suppressing Wnt target genes (Cyclin D1, c-Myc, COX-2). The decrease in p-GSK-3β (Ser9) suggests increased GSK-3β activity, which promotes β-catenin degradation and attenuates Wnt/β-catenin signaling. These indicate that BSF inhibits CRC progression through modulation of the Wnt/β-catenin signaling pathway, promoting apoptosis and suppressing tumor proliferation. This highlights its potential as an adjunct therapy in CRC treatment. In conclusion, these findings suggest that BSF may exert anti-CRC effects by targeting key tumorigenic pathways in preclinical study. Further research, including clinical trials, is needed to confirm its therapeutic potential.

Keywords: Colorectal cancer; BuShenFang; Nude mice; Traditional Chinese Medicine; Subcutaneous Transplanted Tumor; SDG 3 Good health and well-being

1. Introduction

Colorectal cancer (CRC) is one of the most prevalent malignancies worldwide and remains a leading cause of cancer-related mortality [1]. Despite advances in conventional therapies, including surgery, chemotherapy, and targeted agents, treatment resistance and tumor recurrence remain major challenges. Therefore, there is growing interest in exploring alternative and complementary therapeutic strategies, including those derived from Traditional Chinese Medicine (TCM) [2]. Among the cancers, colorectal cancer is of particular concern in this research. As reported by the Malaysia National Cancer Registry from 2012 to 2016, colon cancer ranked first in males (16.9%) and second in females (10.7%) in terms of cancer prevalence. The risk for males to develop colorectal cancer is higher than that for females, especially with increasing age, and the statistics indicate that colon cancer incidence in Malaysia rose for both sexes during that period [3].

BuShenFang (BSF) is a TCM prescription designed for kidney tonifying function [4]. It comprises a mixture of herbal components, including *Pseudobulbus Cremastrae seu Pleiones*, *Fructus akebiae*, *Rehmannia glutinosa*, psoralen, and *Duchesnea indica*. Among these, *Rehmannia glutinosa* and psoralen are traditionally used to invigorate kidney and spleen function, promote yang energy, and support digestive health [5]. The other constituents like *Pseudobulbus Cremastrae seu Pleiones*, *Fructus akebiae*, and *Duchesnea indica* are believed to aid in clearing internal heat, detoxification, resolving carbuncles and improving circulation [6]. Preliminary in vitro studies have shown that BSF exerts anti-CRC activity in human colorectal cancer cell lines, such as HCT116 and SW620 [7]. However, the underlying molecular mechanisms, particularly in vivo, remain poorly understood.

The Wnt/β-catenin signaling pathway plays a pivotal role in CRC development and progression [8]. In normal cells, APC (adenomatous polyposis coli) forms a β-catenin destruction complex with Axin1 and glycogen synthase kinase-3β (GSK-3β). Axin1 serves as a scaffold protein, bringing APC, GSK-3β, and β-catenin into close proximity to facilitate β-catenin phosphorylation and subsequent proteasomal degradation, thus preventing its nuclear accumulation. In CRC, mutations in APC or β-catenin can disrupt this process, leading to cytoplasmic and nuclear accumulation of β-catenin, which subsequently activates downstream oncogenic transcription targets, including c-Myc, Cyclin D1, and COX-2 [9]. Dysregulation of APC, Axin 1 and β-catenin is therefore a hallmark of CRC pathogenesis, and targeting this pathway represents a promising therapeutic approach. Notably, HCT116 cells, which were used in this study, carry β-catenin mutations that prevent its phosphorylation and degradation, resulting in constitutive activation of Wnt/β-catenin signaling. This makes them a suitable model for investigating therapeutic agents that modulate this pathway.

While *in vitro* models offer valuable mechanistic insight, they fail to replicate the complex tumor microenvironment of living organisms. Extended culture of tumor cells can result in genetic drift, phenotypic changes, or contamination, all of which may compromise experimental validity. Therefore, *in vivo* models are crucial for validating the therapeutic potential and biological activity of candidates like BSF under physiologically relevant conditions [10, 11]. To explore the impact of BSF on CRC more thoroughly, multiple groups of mice have been established.

Among *in vivo* platforms, the subcutaneous cell-derived xenograft (CDX) model is widely used due to its simplicity, high tumor formation rate, and reproducibility. In this model, human colorectal cancer cells are injected subcutaneously into immunodeficient nude

mice, allowing for the evaluation of tumor growth and drug response in vivo [12, 13]. Although orthotopic transplantation models more closely mimic metastatic CRC behavior [14-17], the subcutaneous CDX model remains a practical and well-established platform for initial therapeutic screening due to its ease of tumor measurement, consistency, and controlled conditions [18].

Nude mice, due to their T-cell deficiency, serve as a valuable model in oncology research by allowing the engraftment of human tumor cells without immune rejection [19]. This enables the establishment of reliable xenograft models in which human tumors retain key biological characteristics, providing a robust platform for evaluating therapeutic efficacy and drug sensitivity. In this study, a subcutaneous xenograft model was established using HCT116 colorectal cancer cells, which harbor β-catenin mutations leading to aberrant Wnt/β-catenin signaling. Nude mice bearing these tumors were treated with varying concentrations of BSF to evaluate its tumor-inhibitory effects. Tumor growth, histopathology, apoptosis, and key molecular markers in the Wnt signaling pathway were analyzed, offering foundational in vivo evidence for BSF's therapeutic potential in CRC.

2. Materials and methods

2.1. Experimental animals

The animal study was conducted at animal research unit, Shanghai Guangde Traditional Chinese Medicine Clinic. The 16 male nude mice, each 4 weeks old, were housed in a specific pathogen-free (SPF) barrier facility under controlled conditions (temperature: 19–22 °C, relative humidity: 40%–70%, 12-hour light/dark cycle). Animals had free access to standard food and water, and corncob bedding was changed every 4 days. All procedures were performed in accordance with national regulations on animal welfare and were approved by the institutional ethics committee (Approval No. GD2022A-1).

2.2. Main instruments

The main instruments used for sample testing include: biosafety cabinet (sujing antai, Model No. BS-1300IIA2), Super pure water meter (MECK, Model No. Mill-Q Integral5), electronic scales (Mettler Toledo, Model No. ME204E), horizontal shaker (Jiangsu Haimen Qilin Bell instrument, Model No. MICROCL 17), micropipette (GILSON, Model No. KC70239), High current electrophoresis equipment power supply (Bio-Rad, Model No. 1645052), Vertical electrophoresis tank (Bio-Rad, Model No. 1658001), Trough transfer system (Bio-Rad, Model No. 1703930), pH meter (Metter-Toledo GmbH, Germany, Model No. LP115), water bath (Beijing Junyi East Equipment Co., LTD, Model No. JY300),

magnetic stirrer (Beijing Junyi East Equipment Co., LTD, Model No. T8-1), ELISA microplate reader (Biotek, Model No. EPOCH2), centrifugal machine (Thermo, Model No. MICROCL 17), ultrasonic cell disruptor (SONICS, Model No. VCX150), incubator (JINGHONG), Electronic scanner (EPSON, PB4A56180203), Inverted fluorescence Microscope (OLYMPUS, CKX41), Shaker (Thermo Fisher Scientific, 10212432C), Palm centrifuge (Shanghai Hengyi Scientific Instrument Co., LTD).

2.3. Main reagents and consumables

The phosphatase inhibitors (Batch No.: S1873), RIPA Lysis buffer (Batch No.: P0013B), BCA protein concentration determination kit (P0010) and Press cassette (5 x 7 inches) (Batch No.: FFC58) were supplied by Beyotime Biotechnology. The PMSF (Batch No.: ST506), SDS (Batch No.: 30166428) and Tris-base (Batch No.: v900483) were supplied by Sigma Sigma (Shanghai) Trading Co., LTD. The TEMED (Batch No.: 17919) and ECL substrate solution (Batch No.: NCI5079) were supplied by Thermo. The Hcl (Batch No.: 10011018), glycerinum (Batch No.: 10010618), SDS (Batch No.: 10014118), methanol (Batch No.: 10014118), NaCl (Batch No.: 10016318), KCl (Batch No.: 10020318), $Na_2H.12H_2O$ (Batch No.: 10017618), $KHPO_4$ (Batch No.: 10019718) and chloroform (Batch No.: 100006818) were supplied by Sinopharm Group Chemical reagent Co., LTD. The DTT (Batch No.: Amresco0281) and glycine (Batch No.: BL603B) were supplied by Biosharp. The bromophenol blue (Batch No.: BO449-5G), acrylamide (Batch No.: Exp2016109) and Methylacrylamide (Batch No.: Amresc00172) were supplied by Amresco. The Protein marker(14-120KD) (Batch No.: DM111) was supplied by TransGen Biotech. The PVDF membrane (0.45um) (Batch No.: IPVH00010) and PVDF membrane (0.22um) (Batch No.: ISEQ15150) were supplied by Millipore. The developing liquid (Batch No.: 500048-0001), fixative (Batch No.: 500047-0001), isopropanol (Batch No.: A507048), absolute ethyl alcohol (Batch No.: A500737) and DEPC treated water (Batch No.: B501005) were supplied by Sangon Biotech (Shanghai) Co., Ltd. The Crystal violet dye (Batch No.: C0121-500ml), DAPI (Batch No.: C1002) and confining liquid (Batch No.: P0102) were supplied by Beyotime Biotechnology. The Universal Tissue Fixative (neutral) (Batch No.: G1101-500ML) was supplied by Servicebio. The Environmentally friendly dewaxing solution (Batch No.: G1128), Hematoxylin-eosin staining kit (Batch No.: G1076), antifade mounting medium (Batch No.: G1401), EDTA (Batch No.: G1202). The Neutral balsam (Batch No.: 10004160) was supplied by Sinopharm Group Chemical Reagent Co., LTD. The BSA (Batch No.: A600332-0025) was supplied by Sangon Biotech (Shanghai) Co., Ltd. The Tunel (Batch No.: G1501) was supplied by Servicebio. The xStAxVHLL (Batch No.: HY-P5819A) was supplied by MedChemExpress. The APC antibody (Item No.: 19782-1-AP),

COX2/Cyclooxygenase 2/PTGS2 antibody (Item No.: 66351-1-Ig), c-Myc antibody (Item No.: 10828-1-AP), GSK3B antibody (Item No.: 22104-1-AP), Cyclin D1 antibody (Item No.: 60186-1-Ig), AXIN1 antibody (Item No.: 16541-1-AP), Beta Catenin antibody (Item No.: 51067-2-AP) and Phospho-GSK3B(Ser9) antibody (Item No.: 67558-1-lg) were purchased from Proteintech Group, Inc. The GAPDH antibody (Item No.: #5174), mouse IgG(HRP) antibody (Item No.: #7076) and rabbit IgG(HRP) antibody (Item No.: #7074) were purchased from Cell Signaling Technology. The Alexa Fluor 488 Labeled Goat Anti-Rabbit IgG antibody (Item No.: GB25303) was purchased from Servicebio. Slide and cover slip were obtained from Jiangsu Shitai experimental equipment (Item No.: 10212432C). The 1ml RNase-free bagged tips, 200ul RNase-free bagged tips and 10ul RNase-free bagged tips were obtained from EXTRAGENE.

2.4. Experimental methods

2.4.1. Subcutaneous Tumor Model Establishment and Administration Methods

Cell Culture and Passage: The HCT116 cancer cell line (Zhejiang Ruyao Biotechnology Co., Ltd.) was observed under an inverted microscope to assess the degree of confluency and confirm the absence of bacterial or fungal contamination. The culture medium was carefully removed from the bottle. To wash the monolayer cells, phosphate-buffered saline (PBS) was equivalent added to half the volume of the culture medium, typically performing this wash three times. The monolayer cells were digested by adding 1 ml of 0.25% trypsin per 25 cm^2 of surface area. The bottle was gently shaken to ensure that the trypsin coats the cell monolayer, then poured off any excess trypsin. The culture vessel was placed into the incubator and allowed to sit for 2 to 10 minutes. After this incubation, the cells were observed with an inverted microscope to confirm that all cells have been detached and were floating. The side of the bottle was tapped to dislodge any remaining adherent cells. The cells were resuspended in a small volume of culture medium containing fresh serum to inactivate the trypsin, and take 100-200 μl for cell counting. The required number of cells was transferred to a newly labeled culture bottle containing culture medium. Select appropriate culture conditions for the specific cell lines being cultured. This process was repeated according to the growth characteristics of the cell line. Once the cells were in optimal condition and free from contamination, they could be plated and utilized; any surplus could be frozen for future use.

Viable Cell Counting: Viable cell counting involves the use of passaged cells after they have grown into a monolayer. The preparation of the cell suspension began with digestion using 0.25% trypsin, followed by washing with PBS. Subsequently, culture

medium was added, and the mixture was pipetted to prepare the cell suspension for testing. To cover the coverslip, a set of hemocytometers counting chambers was prepared. An appropriate volume of the cell suspension was then drawn into a centrifuge tube, where an equal volume of trypan blue dye was added. This mixture was then placed under a microscope to distinguish between living and dead cells. Note that if the objective was merely to count cells without assessing viability, trypan blue staining was unnecessary. The cell suspension was subsequently dropped onto the counting plate, ensuring that no air bubbles were trapped beneath the coverslip and that the suspension did not flow into adjacent slots. The number of cells in the four large grids was counted. The hemocytometer was placed under a low-power microscope, and the counting board was adjusted until the counting squares were visible. The count was conducted in the four large grids, with each grid containing 16 cells, focusing on the number of unstained cells in the central square. To calculate the number of cells in the original cell suspension and determine cell density, the following formula was employed: (number of cells in cell suspension)/ml = (number of cells in four large grids/4) × 2 × 10^4. \

Tumor Model Establishment in Nude Mice: A total of 16 nude mice aged 5-8 weeks were selected, each weighing approximately 18-20g, and randomly assign them into four groups: Ctrl group (4 mice), L-BSF group (4 mice), H-BSF group (4 mice), and xStAxVHLL group (4 mice).

HCT116 tumor cells in the logarithmic growth phase were harvested and resuspended in sterile DMEM at the cell concentration of 5×10^7 cells/ml, and the inoculation volume was 100 ul. Prior to inoculation, the mice's skin was disinfected using iodophor-soaked cotton balls, applied twice, starting from the ventral side and moving toward the neck, then down to the groin, and finally along the posterior axillary line. For subcutaneous injections, the skin at the back of the neck was gently pinched with the thumb and index finger, while the tail was held with the little finger. Tumor cells were injected subcutaneously into the mid-to-rear region of the forelimb armpit. Inoculations were performed within 30 minutes post-digestion to preserve cell viability, and the cell suspension was kept on ice to minimize metabolic activity. Following inoculation, mice were randomly assigned into four groups (n = 4 per group): control, L-BSF, H-BSF and xStAxVHL. Approximately one week after inoculation, subcutaneous tumor nodules began to appear. Tumor dimensions were measured using a vernier caliper, and volume was calculated using the formula:$V = 1/2 * a * b^2$ (where 'a' represents the long axis and 'b' represents the short axis).

For drug administration, a formulation comprising 15 g of Shanzi mushroom, 9 g of Semen chinensis, 15 g of Rehmannia glutinosa, 12 g of Psoralen, and 15 g of Snakeberry was

decocted in 360 mL of water to yield a stock solution with a concentration of 183 mg/mL. This solution was diluted 7.3 times to achieve a final concentration of 25 mg/mL. For 25 g mice, the target dose was 2.5 mg (100 mg/kg), administered in 100 μL volumes. The control group received an equivalent volume of normal saline via oral gavage. Mice in the L-BSF and H-BSF groups were administered BSF at doses of 100 mg/kg and 200 mg/kg, respectively, via oral gavage five days per week, with two rest days, for a total duration of 3 weeks starting from tumor inoculation. The xStAxVHL group received intraperitoneal injections of 30 mg/kg every other day for six consecutive days, beginning once tumors reached a volume of approximately 50 mm^3.

Throughout the treatment period, body weight and tumor size were measured three times a week. On Day 22 post-inoculation, all mice were sacrificed. Tumors were excised, photographed, and weighed. Portions of the tumor tissue were fixed in formalin for histopathological analysis, while the remaining tissues were frozen for subsequent molecular evaluations.

2.4.2. Immunohistochemical Detection of APC and Ki67 Levels

Tissue samples were first fixed in 10% neutral buffered formalin for 48 hours to preserve morphology. After fixation, the samples were rinsed thoroughly under running water to remove residual fixative and impurities. Dehydration was performed through a graded ethanol series of 50%, 70%, 85%, 95%, and 100% (absolute ethanol), with each step lasting 2 hours. Samples could be stored in 70% ethanol if extended storage was required. Clearing was achieved by immersing tissues in a 1:1 mixture of ethanol and xylene for 2 hours, followed by two successive immersions in pure xylene for 2 hours each. Tissues were then infiltrated in a 1:1 mixture of xylene and molten paraffin for 1–2 hours and further embedded in molten paraffin in two separate containers for approximately 3 hours each to ensure complete infiltration. The paraffin-saturated tissues were embedded in a mold, oriented properly, and allowed to solidify. Excess wax was trimmed from the paraffin blocks, which were subsequently mounted on a microtome. Sections were cut at a thickness of 4–7 μm using a rotary microtome with the blade angled at 5° to the tissue surface.

For staining, paraffin sections were dewaxed using three successive immersions in environmentally friendly dewaxing solutions I, II, and III for 10 minutes each. This was followed by rehydration in absolute ethanol I, II, and III for 5 minutes each and then rinsed in distilled water. Antigen retrieval was performed by placing the slides in EDTA buffer (pH 6.0), ensuring the buffer volume was sufficient to prevent drying. After natural cooling, slides were rinsed in PBS (pH 7.4) three times for 5 minutes each on a destaining shaker. Sections

were then encircled with a hydrophobic barrier using a histochemistry pen and blocked with bovine serum albumin (BSA) for 30 minutes. The primary antibody APC/Ki67 was added dropwise, and the slides were incubated overnight at 4°C in a humidified chamber. The next day, sections were washed three times with PBS (pH 7.4), 5 minutes per wash, followed by incubation with the appropriate HRP-conjugated secondary antibody for 50 minutes at room temperature in the dark. After a further three washes in PBS (5 minutes each), DAB chromogenic reagent was applied dropwise within the marked area. Color development was monitored under a microscope, with brown staining indicating a positive signal. The reaction was stopped by rinsing with tap water. Counterstaining was carried out with hematoxylin for 3 minutes, followed by differentiation in a brief dip of differentiation solution and rinsing with tap water until nuclei appeared blue. Dehydration was performed through graded alcohols (75%, 85%, absolute ethanol I and II, 5 minutes each), cleared in n-butanol for 5 minutes, then xylene I for 5 minutes. After air drying, the sections were mounted with coverslips using a suitable mounting medium and examined under a light microscope for image capture and analysis.

2.4.3. Tissue Apoptosis detected by TUNEL

Paraffin-embedded tissue sections were first dewaxed by immersing them sequentially in xylene I for 10 minutes, xylene II for 10 minutes, and again in xylene II for an additional 10 minutes. This was followed by rehydration through a graded ethanol series using absolute ethanol I, II, and III for 5 minutes each. Finally, the sections were rinsed with distilled water. Longer dewaxing times may be required under lower ambient temperatures to ensure complete paraffin removal. After slight drying, a hydrophobic barrier was drawn around the tissue using a histochemistry pen to confine the reagents. Proteinase K working solution (prepared at a 1:9 ratio of stock solution to PBS) was added to cover the tissue and incubated at 37 °C for 22 minutes. Slides were then washed three times in PBS (pH 7.4) for 5 minutes each using a decolorizing shaker. Once slightly dried again, membrane rupture working solution was applied within the marked area and incubated at room temperature for 20 minutes, followed by three PBS washes (5 minutes each). Equilibration buffer was then added dropwise and incubated at room temperature for 10 minutes. For the TUNEL reaction, a labeling solution was freshly prepared by mixing TDT enzyme, dUTP, and reaction buffer in a 1:5:50 ratio. The mixture was applied to cover the tissue, and the slides were incubated in a humidified chamber at 37 °C for 2 hours to allow for labeling of apoptotic cells. Following incubation, the slides were rinsed with PBS three times for 5 minutes each. DAPI staining solution was then applied to the sections, followed by a 10-minute incubation at room temperature in the dark. After another set of PBS washes (3 × 5 minutes), excess liquid

was gently removed, and the sections were mounted with an anti-fluorescence quenching mounting medium. The stained sections were observed under a fluorescence microscope. DAPI-stained nuclei were visualized as blue signals (excitation: 330–380 nm; emission: 420 nm), whereas FITC-labeled apoptotic cells exhibited green fluorescence (excitation: 465–495 nm; emission: 515–575 nm).

2.4.4. Immunofluorescence detects the β-catenin

For staining, paraffin-embedded sections were dewaxed by sequential immersion in three changes of environmentally friendly dewaxing solution (I, II, and III) for 10 minutes each. This was followed by rehydration in absolute ethanol I, II, and III, each for 5 minutes, and a final rinse in distilled water. Antigen retrieval was performed by immersing the slides in EDTA buffer (pH 6.0), ensuring the sections remained moist and avoiding excessive evaporation. After natural cooling, the slides were transferred to PBS (pH 7.4) and gently agitated on a destaining shaker for 5 minutes, repeated three times. After slight drying, a hydrophobic barrier was drawn around the tissue using a histochemistry pen. The sections were blocked with bovine serum albumin (BSA), which was applied dropwise and incubated for 30 minutes at room temperature. Subsequently, the primary antibody (prepared as described above) was added to cover the tissue, and the slides were incubated flat in a humidified chamber overnight at 4 °C. After incubation, the slides were washed three times in PBS (pH 7.4) for 5 minutes each on a shaker. The corresponding secondary antibody (dilution ratio as listed in the table above) was then applied, and the slides were incubated at room temperature for 50 minutes in the dark. After another set of PBS washes (3 × 5 minutes), DAPI staining solution was added and incubated for 10 minutes at room temperature in the dark. The slides were again washed three times with PBS, excess liquid was removed, and the sections were mounted using an anti-fluorescence quenching mounting medium. The stained sections were then observed and imaged under a fluorescence microscope.

2.4.5. Western Blot detects protein levels downstream of the Wnt/β-catenin signaling pathway

An appropriate amount of tumor tissues from xenografted HCT116 colorectal cancer tumors was placed into a 1.5 mL grinding tube, and a suitable volume of lysis buffer was added. The sample was incubated on ice for 30 minutes before being homogenized using a tissue grinder. The homogenate was then sonicated in an ice bath using an ultrasonic crusher at 25% power for 1 second, followed by a 1-second pause, repeated for a total of 10 cycles to prevent protein degradation. The lysate was centrifuged at 13,000 rpm for 10 minutes at

4 °C, and the resulting supernatant was carefully transferred to a new tube, avoiding any lipid layer floating on top.

For protein quantification, each sample (4 μL) was diluted with 16 μL PBS (5× dilution). Bradford standards were prepared at concentrations of 0.00, 0.125, 0.25, 0.5, 0.75, 1.00, and 1.5 mg/mL and loaded into a 96-well plate along with sample dilutions and blank controls. Each well contained 5 μL of sample or standard and 250 μL of Coomassie Brilliant Blue G-250 staining solution. Bubbles were avoided during pipetting to prevent interference. Absorbance was measured within 2 hours. A standard curve was generated based on OD values, and sample protein concentrations were calculated accordingly.

For protein denaturation, the protein supernatant was mixed with 5× SDS-PAGE loading buffer (250 mM Tris-HCl pH 6.8, 10% SDS, 50% glycerol, 0.5 M DTT, and 0.05% bromophenol blue) and boiled for 10 minutes. SDS-PAGE gels were prepared by assembling clean and dry glass plates. The separation gel was poured, overlaid with absolute ethanol, and allowed to polymerize. Once solidified, the ethanol was discarded, and the gel was rinsed and dried. The stacking gel was then added, and a comb was inserted. After polymerization, the comb was removed, and the gel was mounted in an electrophoresis tank filled with running buffer. A total of 20 μg of each protein sample, along with a molecular weight marker, was loaded into the wells. Electrophoresis was performed at 80 V until the bromophenol blue reached the interface between stacking and separation gels, followed by 100 V until the dye front reached the bottom (~1.5 hours).

The gel was excised, and the band of interest was identified using the marker. A PVDF membrane and filter paper were cut to match the gel size. The membrane was activated in methanol and then equilibrated in transfer buffer. The transfer sandwich was assembled in the order: black plate, fiber pad, filter paper, gel, PVDF membrane, filter paper, fiber pad, and white plate. The assembly was placed in the transfer apparatus with the black plate aligned to the negative electrode, and the transfer was performed at 100 V for 60 minutes in an ice bath.

For immunodetection, the membrane was blocked in TBST containing 5% skimmed milk for 40 minutes at room temperature with gentle shaking. The appropriate primary antibody, diluted in antibody diluent, was applied, and the membrane was incubated overnight at 4 °C. After three washes in TBST (5 minutes each), the membrane was incubated with HRP-conjugated secondary antibody (1:20,000 in TBST) at 37 °C for 1 hour. Following another three washes, enhanced chemiluminescence (ECL) working solution was prepared by mixing the enhancer and stable peroxidase solution in a 1:1 ratio. The membrane was

incubated with this solution until fluorescent bands appeared. Excess substrate was removed with filter paper, and the membrane was covered with cling film. X-ray film was placed on top, and the blot was developed and fixed using standard developer and fixer solutions.

2.5. Statistical analysis

The experimental data were analyzed using SPSS version 27.0 statistical software. GraphPad Prism version 9.0 was utilized for graphical representation. The experimental data are expressed as mean ± standard deviation (x ± SD). Independent samples t-test was used to determine whether there is a significant difference between two groups. One-way analysis of variance (ANOVA) was employed for comparisons of more than 2 groups to determine statistical significant differences. Post-hoc Dunnet's test was used to compare groups with the control group when there is a significant difference. A p-value of 0.05 indicates a statistically significant difference, among which * vs Ctrl $p < 0.05$, ** vs Ctrl $p < 0.01$, *** vs Ctrl $p < 0.001$, # vs xStAxVHLL $p < 0.05$, ## vs xStAxVHLL $p < 0.01$, ### vs xStAxVHLL $p < 0.001$.

3. Results

3.1. BuShenFang inhibits the growth of HCT116 transplanted tumors in nude mice

HCT116 cells were subcutaneously inoculated into nude mice, and drug treatment commenced once the tumors reached approximately 50 mm^3. Tumor growth was then monitored throughout the treatment period until tumors approached the humane endpoint (approximately 800–1000 mm^3). Body weight and tumor size were measured three times a week. After 22 days, the nude mice were sacrificed. Tumor images were captured (Figure 1), and their weights were recorded (Figure 2). The average volume of the transplanted tumors in nude mice was calculated, and a volume change curve for the mice with transplanted tumors was generated (Figure 3). Throughout the treatment period, the tumor volume in each group of nude mice gradually increased with the duration of administration; however, the tumor volume post-treatment in each group was smaller than that of the control group ($p < 0.001$). Following treatment, each nude mouse was sacrificed, and tumor tissue samples were collected and weighed, leading to the creation of a histogram of tumor weights (Figure 3). Compared to the control group, the average tumor weight in the L-BSF, H-BSF, and xStAxVHLL groups was significantly reduced ($p < 0.05$). The results indicate that different concentrations of BSF can inhibit tumor growth in a dose-dependent manner. Compared with the xStAxVHLL group, the average tumor weight of nude mice in the L-BSF group and H-

BSF group increased ($p<0.05$). In conclusion, BSF effectively inhibits the growth of subcutaneously transplanted tumors in nude mice.

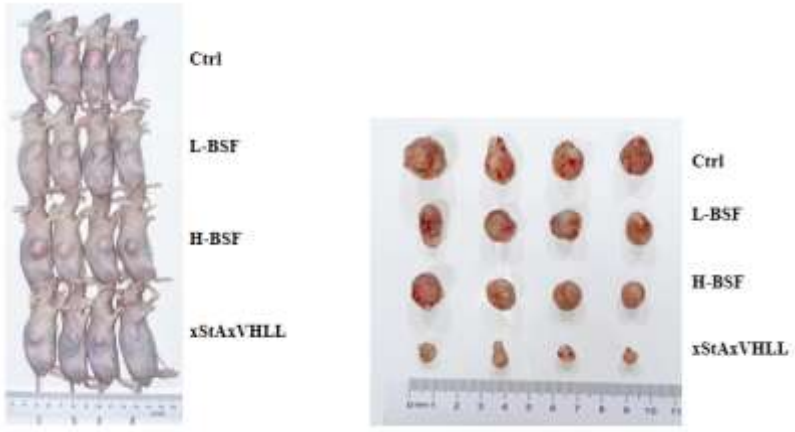

Figure 1. Pictures of nude mice with transplanted tumors in each group.

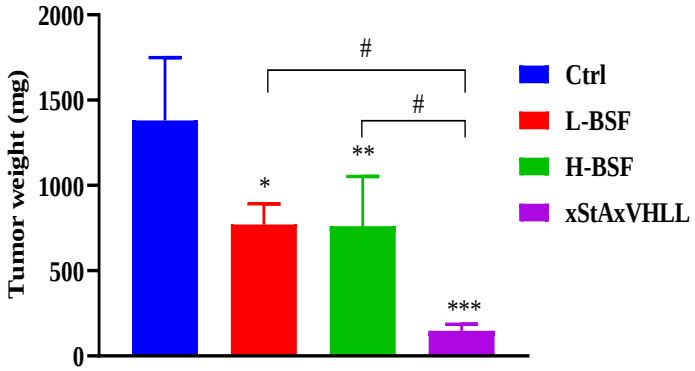

Figure 2. Effect of BuShenFang on the body weight of nude mice with transplanted tumors. * vs Ctrl $p < 0.05$; ** vs Ctrl $p < 0.01$; *** vs Ctrl $p < 0.001$; # vs xStAxVHLL $p < 0.05$.

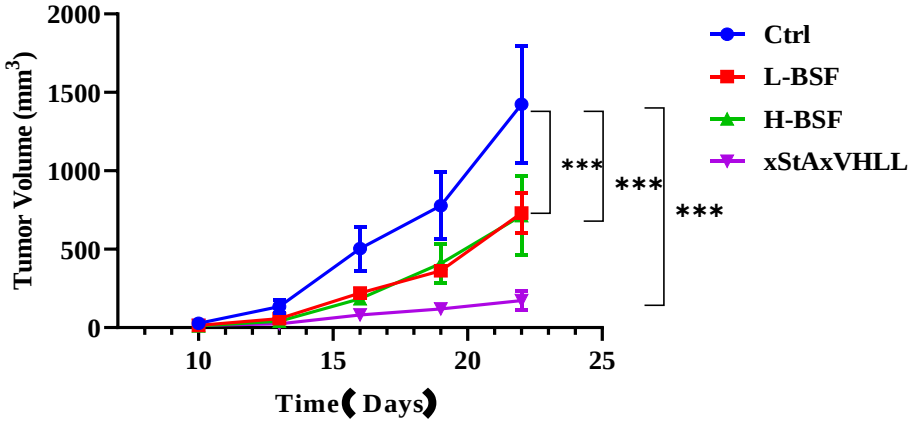

Figure 3. Effect of BuShenFang on volume changes of transplanted tumors in nude mice. *** vs Ctrl $p < 0.001$.

3.2. BuShenFang inhibits the expression of KI67 in tumor tissues of nude mice with HCT116 transplanted tumors

Immunohistochemical analysis was conducted to evaluate the expression of the proliferation-related nuclear antigen Ki67 in tumor tissues from nude mice treated with kidney-tonifying drugs at various concentrations. Ki67 protein was positively expressed in all groups, with positively stained nuclei appearing brown and diffusely distributed throughout the tissue. However, tumor tissues from the L-BSF, H-BSF, and xStAxVHLL exhibited predominantly weak to moderate Ki67 expression, in contrast to the strong positive expression observed in the control group (Figure 4). This reduction in Ki67 expression suggests that BuShenFang treatment suppresses tumor cell proliferation in a dose-dependent manner.

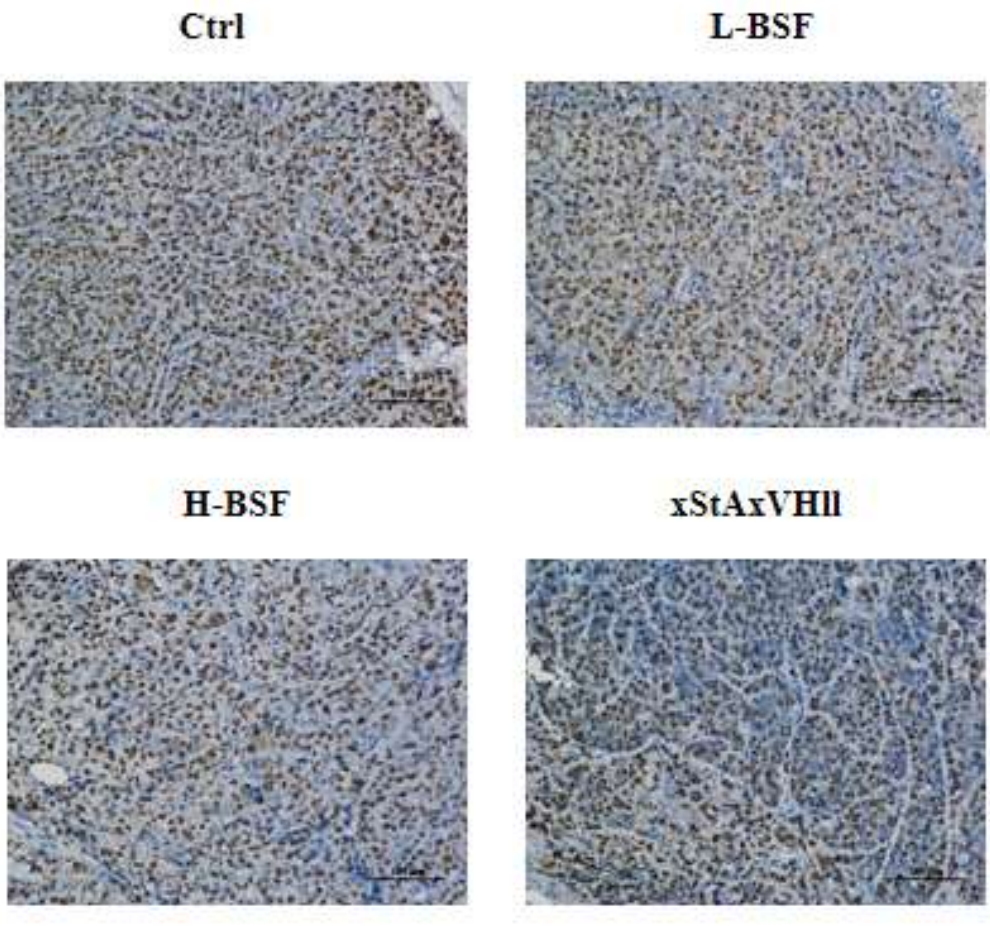

Figure 4. Effect of BuShenFang on KI67 expression in tumor tissue of nude mice with transplanted tumors (100X). Brown-stained nuclei indicate Ki67-positive cells, which are markers of active cell proliferation. Representative images show reduced Ki67 expression in treatment groups (L-BSF, H-BSF, and xStAxVHLL) compared to the control group.

3.3. BuShenFang promotes apoptosis in the tumor tissue of HCT116 transplanted nude mice

TUNEL staining was utilized to assess the impact of BSF on apoptotic changes in the tumor tissue of these mice. The results indicated that, in comparison to the Ctrl group, the level of apoptosis in the tumor tissue of nude mice increased in the L-BSF group, H-BSF group, and xStAxVHLL group (Figure 5).

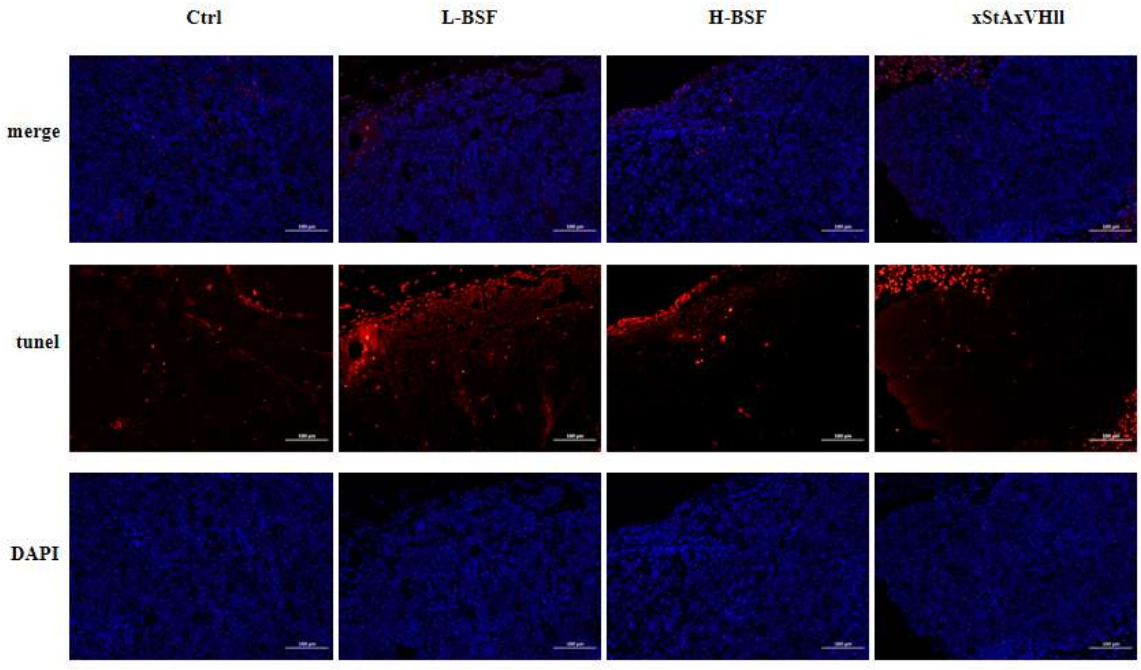

Figure 5. The effect of BuShenFang on apoptosis in the tumor tissue of nude mice with transplanted tumors (100X).

3.4. BuShenFang reduces the expression of β-catenin in the tumor tissues of nude mice with HCT116 transplanted tumors

β-catenin is a central effector of the Wnt signaling pathway, whose nuclear accumulation promotes the transcription of oncogenes such as Cyclin D1 and c-Myc, driving colorectal tumorigenesis. Aberrant β-catenin expression is frequently observed in CRC due to upstream mutations in regulatory proteins like APC. In this study, immunofluorescence was used to assess the β-catenin levels in tumor tissues from BSF-treated mice. Immunofluorescence results revealed that, in the tumor tissues of nude mice with transplanted tumors, the expression of β-catenin was diminished in the L-BSF group, H-BSF group, and xStAxVHLL group compared to the Ctrl group (Figure 6). These findings strongly suggest that BSF can down-regulate β-catenin protein levels in vivo in nude mice with transplanted tumors.

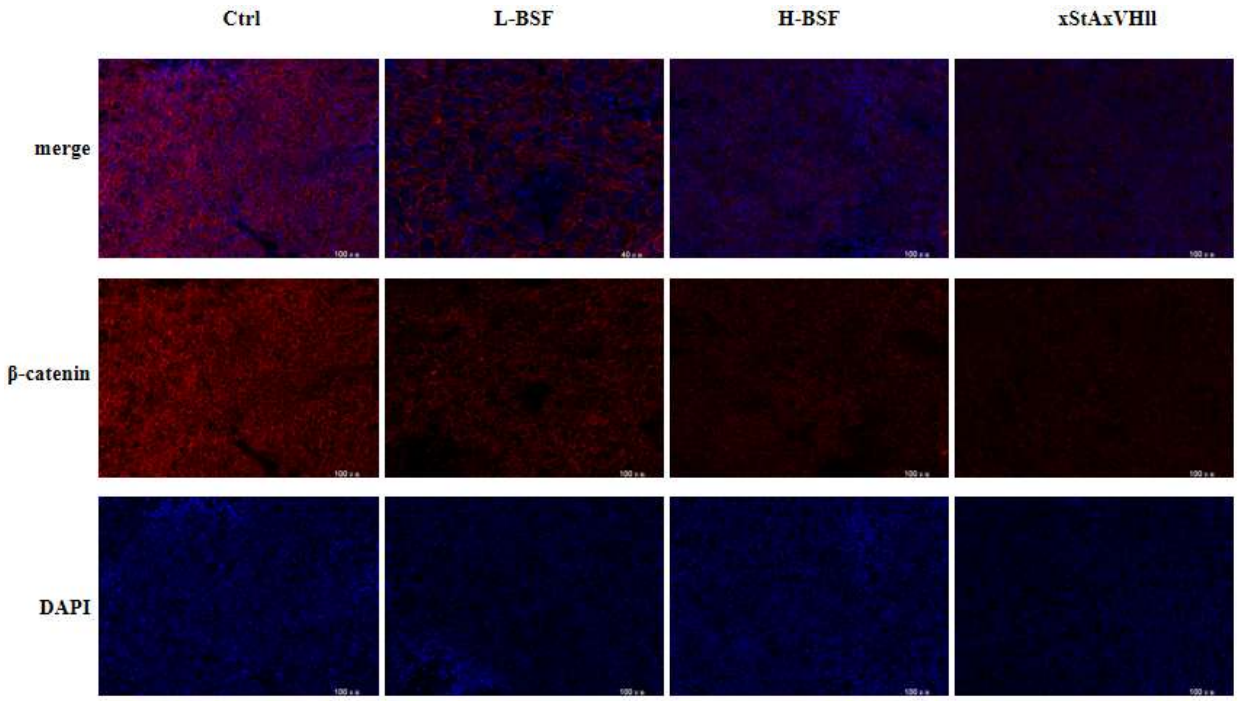

Figure 6. demonstrates the effect of BuShenFang on β-catenin expression in the tumor tissue of nude mice with HCT116 transplanted tumors (100X).

3.5. Effect of BuShenFang on Wnt Signaling Pathway-Related Molecules in Tumor Tissues of Nude Mice with HCT116 Transplanted Tumors

The Wnt/β-catenin signaling pathway is one of the most frequently dysregulated pathways in colorectal cancer, often due to mutations or altered expression of APC, β-catenin, GSK-3β, and Axin1. Aberrant activation of this pathway enhances tumor proliferation, survival, and metastasis through transcriptional upregulation of downstream targets such as c-Myc, Cyclin D1, and COX-2. To investigate whether BSF exerts anti-tumor effects by modulating this signaling cascade, the protein expression levels of key upstream and downstream molecules were assessed using Western blotting.

The results presented in Figure 7 indicated that, compared to the Ctrl group, the APC protein levels in the tumor tissue cells of the L-BSF group, H-BSF group, and xStAxVHLL group were significantly elevated ($p < 0.05$). Conversely, in the H-BSF group and xStAxVHLL group, significant decreases in β-catenin, p-GSK-3β/GSK-3β, and Axin1 levels were observed compared to the Ctrl group ($p < 0.05$). In comparison to the xStAxVHLL group, the levels of APC and Axin1 in the L-BSF group were statistically significant ($p < 0.01$), whereas β-catenin and p-GSK-3β/GSK-3β did not show statistical significance ($p > 0.05$). No statistically significant differences were observed for APC, β-catenin, p-GSK-3β/GSK-3β, and Axin1 in the H-BSF group ($p > 0.05$).

Although Axin1 expression was reduced following BSF treatment, APC was upregulated, while β-catenin and its downstream oncogenic targets (c-Myc, Cyclin D1, and COX-2) were downregulated. This indicates that BSF may inhibit the Wnt/β-catenin pathway through mechanisms that are not strictly dependent on Axin1. The increase in APC expression, combined with decreased p-GSK-3β/GSK-3β levels, may compensate for Axin1 reduction and facilitate β-catenin degradation. Thus, despite lower Axin1 levels, the overall effect of BSF is suppressive toward Wnt/β-catenin signaling and tumor progression.

Further analysis of downstream targets showed that c-Myc, Cyclin D1, and COX-2 protein levels were reduced to varying degrees. In comparison to the Ctrl group, the protein levels of c-Myc, Cyclin D1, and COX-2 in the L-BSF group exhibited a downward trend ($p > 0.05$). Conversely, the protein levels of c-Myc, Cyclin D1, and COX-2 in the H-BSF group and the xStAxVHLL group were significantly reduced compared to the Ctrl group ($p < 0.05$). Additionally, c-myc in the L-BSF group was statistically significant when compared to the xStAxVHLL group ($p < 0.01$), while CyclinD1 and COX-2 exhibited no statistical significance ($p > 0.05$). In the H-BSF group, CyclinD1, c-myc, and COX-2 also did not show statistical significance ($p > 0.05$). Overall, these findings suggest that H-BSF can significantly regulate the Wnt signaling pathway.

(a)

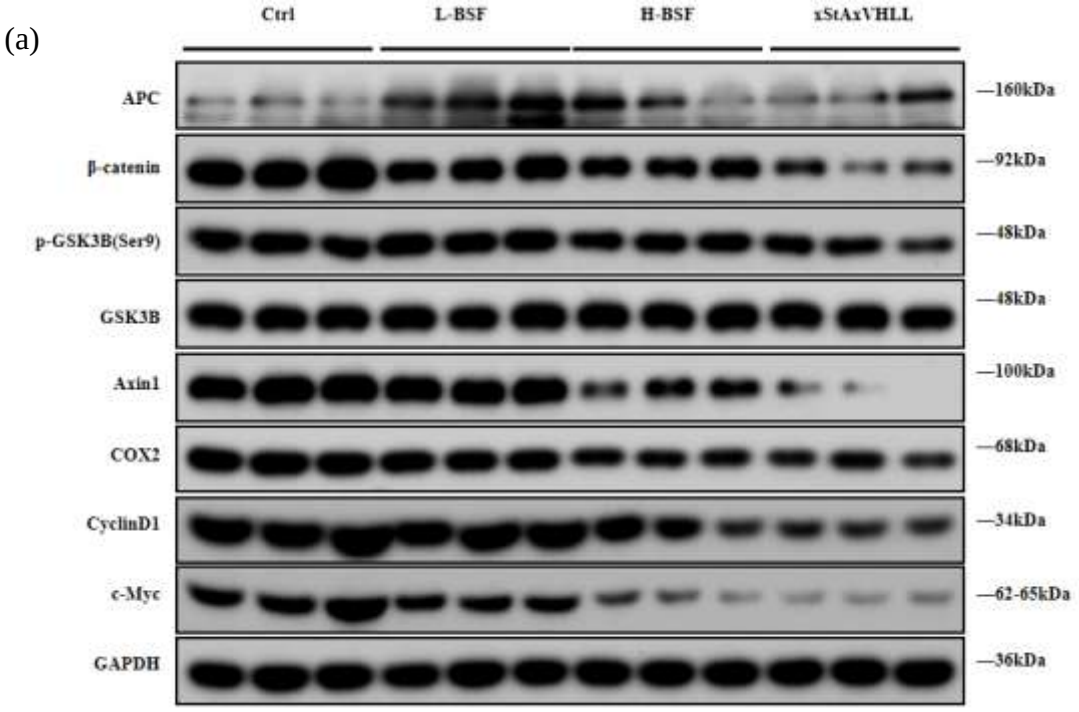

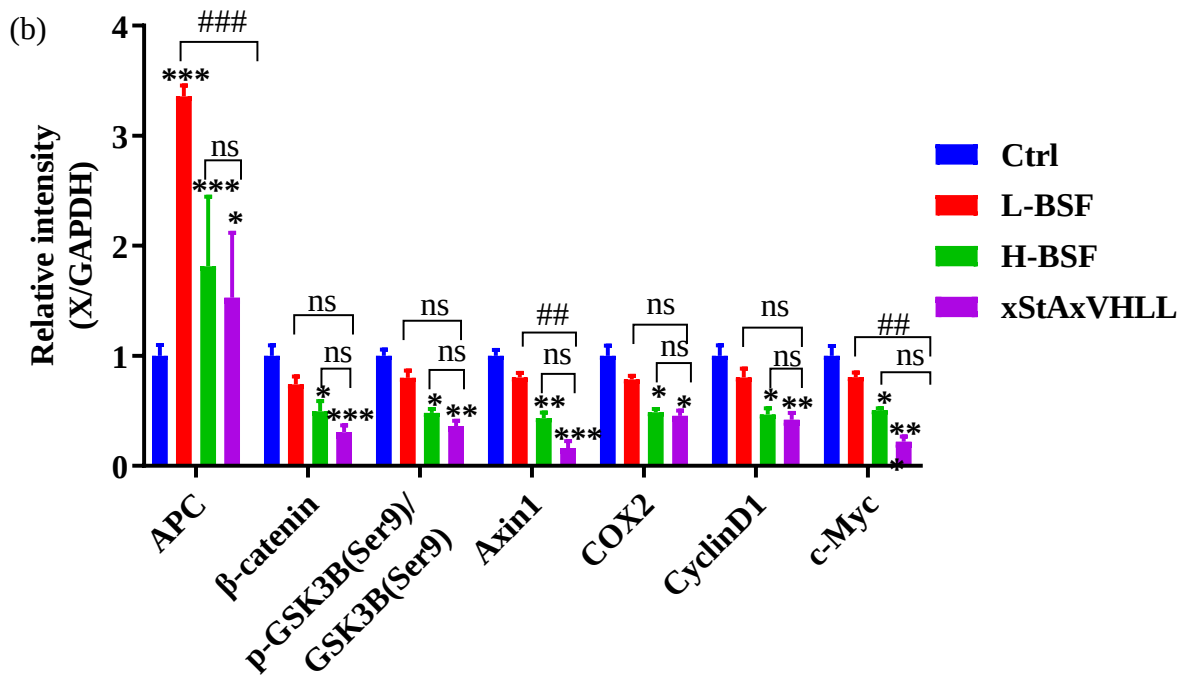

Figure 7. (a) Western blot analysis and (b) relative band intensity showing the effect of BuShenFang on Wnt signaling pathway in tumor tissue of HCT116 transplanted nude mice. * vs Ctrl $p < 0.05$; ** vs Ctrl $p < 0.01$; *** vs Ctrl $p < 0.001$; ## vs xStAxVHLL $p < 0.01$; ### vs xStAxVHLL $p < 0.001$.

4. Discussion

Currently, various tumor animal models have been developed, which can be broadly categorized into chemically induced tumor models, transgenic tumor models, and transplanted tumor models [20]. Among these, the transplanted tumor model is the most frequently utilized animal model for studying CRC due to its high metastasis rate and ability to express specific characteristics needed for experimental studies.

Transplantation tumor animal models can be categorized into syngeneic transplantation and xenotransplantation [21]. Syngeneic transplantation involves inoculating mouse tumor cells and tissues into mice that share the same genetic background. This model is less susceptible to rejection and facilitates the evaluation of the relationship between the tumor and its microenvironment; however, it is genetically distinct from human tumors [22]. Conversely, xenografting entails transplanting human tumor cells or tissues into immunodeficient mice [23]. Despite the absence of an immune response in these mice and the low survival rates of transplants, this model is widely employed in human cancer research [24].

In this study, a subcutaneous xenograft tumor model was established by subcutaneously inoculating BALB/c nude mice (aged 3 to 5 weeks) with 5×10^6 HCT116 cells suspended in 0.2 ml PBS per mouse. Tumors began to form within three weeks, reaching an approximate diameter of 1 cm, with a tumor formation rate of 100%. After 10 weeks of growth, no liver or lymph node metastases were observed [25], consistent with previous observations that subcutaneous tumor models typically lack metastatic potential due to their ectopic implantation site [26]. Despite this limitation, subcutaneous models remain useful for studying solid tumor growth, evaluating biomarker expression and therapeutic efficacy [27, 28].

Furthermore, logarithmically growing HCT-116 cells were inoculated subcutaneously into nude mice, measuring tumor size three times a week and observing them continuously for five weeks. The tumor growth conditions were generally consistent with findings reported in the literature [29]. A tumor growth curve was constructed based on the measured data, indicating that tumor size exhibited close to exponential growth, suggesting that the tumor cells were in a stable state of division within the subcutaneous microenvironment. Upon reaching a tumor volume of 100 cm^3, the medium-dose and high-dose groups received varying concentrations of BSF via gavage once daily, administering 0.2 ml each, while the control group was given an equivalent volume of normal saline. The administration regimen consisted of oral dosing, with treatment occurring five days on and two days off per week. The results demonstrated that the tumor volume and weight ratios of mice in the L-BSF group, H-BSF group, and xstaxvhl group were significantly lower than those in the control group, indicating that all treatments effectively inhibited the growth of transplanted tumors and exhibited notable therapeutic effects.

The KI67 immunohistochemical staining was also performed on tumor tissues, revealing that both the BSF group and the xstaxvhl group effectively inhibited tumor cell proliferation through the regulation of KI67. TUNEL staining results indicated that these groups promoted tumor cell apoptosis. Lin et al. [30] established a transplanted tumor mouse model by subcutaneously injecting CT26 cells, demonstrating that WTX treatment significantly reduced tumor weight in this xenografted model. Immunohistochemical analysis showed a reduction in the positive area of KI67. Similarly, Hu et al. [31] constructed a transplanted mouse model using HCT116 cells and treated it with ursolic acid (UA) from days 6 to 22. Their findings indicated that administration of UA (12.5 mg/kg daily) or (10 mg/kg for 5 consecutive days) significantly decreased tumor weight, size, and volume. Furthermore, the area of tumor cell apoptosis increased, and KI67 expression was significantly lower compared to the control group. The results from this portion of the

experimental mechanism study showed that, relative to the Ctrl group, APC protein levels in intestinal tumor tissue cells in the H-BSF group were significantly elevated, while levels of β-catenin, p-GSK-3β/GSK-3β, and Axin1 proteins were significantly reduced. Additionally, the downstream target genes of the β-catenin signaling pathway, including CyclinD1, c-Myc, and COX-2, exhibited significantly lower histone levels in the H-BSF group.

Genome-wide expression analysis reveals that the inhibition of the Wnt/β-catenin signaling pathway is a crucial mediator of the anti-cancer and chemotherapy-sensitizing effects of Andrographis paniculata in a previous study [32]. The findings of this study demonstrate that BSF effectively inhibits tumor growth in subcutaneously transplanted HCT116 tumors in nude mice, primarily through modulation of the Wnt/β-catenin signaling pathway. These results align with existing literature, which highlights the therapeutic potential of TCM formulations in CRC. For instance, Andrographis paniculata has been shown to inhibit β-catenin nuclear localization and downstream target expression, enhancing chemotherapy sensitivity [32]. Similarly, ginsenosides such as Rg3 have demonstrated anti-tumor effects by downregulating β-catenin and promoting apoptosis in CRC models [24]. The findings also resonate with research on the Guben Xiaoai Recipe, which modulates Wnt/β-catenin signaling to inhibit tumor glycolysis and proliferation. However, BSF's notable impact on APC expression and its dose-dependent effects suggest a unique and potentially synergistic mechanism compared to these formulations. This underscores BSF's promise as a therapeutic agent, particularly given its comprehensive modulation of key signaling molecules like APC, β-catenin, and Cyclin D1. While the study provides valuable insights, further comparisons with clinically established formulations and human trials are necessary to fully contextualize BSF's efficacy and potential application in CRC treatment.

Based on these findings, this study concluded that high-dose BSF inhibited the expression of proteins associated with the Wnt/β-catenin signaling pathway by increasing APC levels, thereby suppressing the proliferation of tumor cells in nude mice with HCT116 tumor transplants, promoting cancer cell apoptosis, and consequently inhibiting tumor tissue growth [33]. While the findings highlight the potential of BSF as a therapeutic agent against CRC, several limitations warrant critical consideration. The study relies predominantly on a subcutaneous xenograft model, which, while effective for assessing tumor growth and drug effects, does not fully replicate the tumor microenvironment or metastatic behavior seen in human CRC [34]. Alternative models, such as orthotopic transplantation or PDX, could provide more clinically relevant insights. Furthermore, while the study focuses on the Wnt/β-catenin signaling pathway, CRC is a heterogenous disease influenced by multiple pathways, including PI3K/AKT and MAPK signaling, which might also contribute to BSF's effects.

Exploring these alternative mechanisms using transcriptomic or proteomic analyses could uncover broader molecular impacts [35]. Additionally, the complex composition of BSF poses challenges in identifying the active constituents and their individual contributions to the observed effects. Employing fractionation and bioactivity-guided isolation could clarify these roles [36]. Finally, the lack of clinical correlation limits the translational impact, necessitating further validation through human trials to substantiate the relevance of these findings. Addressing these limitations could strengthen the understanding of BSF's mechanisms and its potential therapeutic value.

5. Conclusion

The research findings presented confirm the inhibitory effect of BSF on subcutaneously transplanted HCT116 tumors in nude mice. Furthermore, the results demonstrate that BSF reduces c-Myc levels by inhibiting the activation of the Wnt/β-catenin signaling pathway, subsequently blocking the expression of its downstream target genes, including c-Myc, cyclin D1, and COX-2. This reduction in expression can inhibit the proliferation of tumor cells in mice with subcutaneous transplanted tumors and promote their apoptosis, contributing to advancements in cancer prevention and treatment in alignment with the United Nations Sustainable Development Goal (SDG) 3: Good Health and Well-being.

Author Contributions: Conceptualization: JJ and KBL. Formal analysis: KWG, JJ, XG and HKSY. Investigation: KWG, JJ, XG and HKSY. Writing – original draft preparation: JJ, XG, LBVS and HKSY. Writing – review and editing: PEK, SKL,AKJ and LCM. Validation: PEK, SKL,AKJ and LCM. Supervision: KBL. Funding acquisition: KWG and KBL.

Funding: This work was not supported by any funding agency.

Conflicts of Interest: The authors declare no conflict of interest.

References

1. Wang M, Zheng C, Wang Z, *et al*. Colorectal cancer: highlight the clinical research current progress. Holistic Integr Oncol 2025; 4(1): 17.
2. Ji J, Phang HC, Gu X, *et al*. A Review on Colorectal Cancer and the Role of Traditional Chinese Herbal Medicine as Complementary Therapy. Prog Microbes Mol Biol 2024; 7(1).
3. Wong Y, Subramaniam H, Ling Shing W, *et al*. Green synthesis and characterization of CuO/ZnO nanocomposite using Musa acuminata leaf extract for cytotoxic studies on colorectal cancer cells (HCC2998). Green Process Synth 2024; 13: 20240164.
4. Goh KW, Ji J, Gu X, *et al*. Modulation of Wnt/β-Catenin Signaling Pathway by Bushenfang for Colorectal Tumor Inhibition in mice with Adenomatous Polyposis Coli Gene Mutation. Prog Microbes Mol Biol 2025; 8(1).
5. Zhang RX, Li MX, Jia ZP. Rehmannia glutinosa: review of botany, chemistry and pharmacology. J Ethnopharmacol 2008; 117(2): 199-214.

6. Wang J, Wu M, Liu J, *et al*. An integrated strategy for quality control of Pseudobulbus Cremastrae seu Pleiones based on Q-marker. J Chromatogr A 2024; 1730: 465105.
7. Goh KW, Ji J, Phang H, *et al*. Mechanistic Insights into the Inhibition of Colorectal Cancer by BuShenFang through Adenomatous Polyposis Coli Expression and Wnt/β-catenin Pathway Regulation. Prog Microbes Mol Biol 2025; 8.
8. He K and Gan WJ. Wnt/β-Catenin Signaling Pathway in the Development and Progression of Colorectal Cancer. Cancer Manag Res 2023; 15: 435-448.
9. Shang S, Hua F, Hu ZW. The regulation of β-catenin activity and function in cancer: therapeutic opportunities. Oncotarget 2017; 8(20): 33972-33989.
10. Callaway E. Contamination hits cell work. Nature 2014; 511(7511): 518.
11. ASN-0002 ATCCSDOW. Cell line misidentification: the beginning of the end. Nat Rev Cancer 2010; 10(6): 441-8.
12. Liu M, Zhao G, Zhang D, *et al*. Active fraction of clove induces apoptosis via PI3K/Akt/mTOR-mediated autophagy in human colorectal cancer HCT-116 cells. Int J Oncol 2018; 53(3): 1363-1373.
13. Lee MS, Helms TL, Feng N, *et al*. Efficacy of the combination of MEK and CDK4/6 inhibitors in vitro and in vivo in KRAS mutant colorectal cancer models. Oncotarget 2016; 7(26): 39595-39608.
14. Fidler IJ. Orthotopic implantation of human colon carcinomas into nude mice provides a valuable model for the biology and therapy of metastasis. Cancer Metastasis Rev 1991; 10(3): 229-43.
15. Lupu CM, Eisenbach C, Lupu AD, *et al*. Adenoviral B7-H3 therapy induces tumor specific immune responses and reduces secondary metastasis in a murine model of colon cancer. Oncol Rep 2007; 18(3): 745-8.
16. Donigan M, Loh BD, Norcross LS, *et al*. A metastatic colon cancer model using nonoperative transanal rectal injection. Surg Endosc 2010; 24(3): 642-7.
17. Céspedes MV, Espina C, García-Cabezas MA, *et al*. Orthotopic microinjection of human colon cancer cells in nude mice induces tumor foci in all clinically relevant metastatic sites. Am J Pathol 2007; 170(3): 1077-85.
18. Ye F, Chen C, Qin J, *et al*. Genetic profiling reveals an alarming rate of cross-contamination among human cell lines used in China. Faseb J 2015; 29(10): 4268-72.
19. Flatmark K, Maelandsmo GM, Martinsen M, *et al*. Twelve colorectal cancer cell lines exhibit highly variable growth and metastatic capacities in an orthotopic model in nude mice. Eur J Cancer 2004; 40(10): 1593-8.
20. Tong Y, Yang W, Koeffler HP. Mouse models of colorectal cancer. Chin J Cancer 2011; 30(7): 450-62.
21. Oh BY, Hong HK, Lee WY, *et al*. Animal models of colorectal cancer with liver metastasis. Cancer Lett 2017; 387: 114-120.
22. Khanna C and Hunter K. Modeling metastasis in vivo. Carcinogenesis 2005; 26(3): 513-23.
23. Saxena M and Christofori G. Rebuilding cancer metastasis in the mouse. Mol Oncol 2013; 7(2): 283-96.
24. He BC, Gao JL, Luo X, *et al*. Ginsenoside Rg3 inhibits colorectal tumor growth through the down-regulation of Wnt/ß-catenin signaling. Int J Oncol 2011; 38(2): 437-45.

25. Fu XY, Besterman JM, Monosov A, *et al*. Models of human metastatic colon cancer in nude mice orthotopically constructed by using histologically intact patient specimens. Proc Natl Acad Sci U S A 1991; 88(20): 9345-9.
26. Kubota T. Metastatic models of human cancer xenografted in the nude mouse: the importance of orthotopic transplantation. J Cell Biochem 1994; 56(1): 4-8.
27. Kang KJ, Pyo JH, Ryu KJ, *et al*. Oncogenic Role of BOLL in Colorectal Cancer. Dig Dis Sci 2015; 60(6): 1663-73.
28. Wang W, Kim SH, El-Deiry WS. Small-molecule modulators of p53 family signaling and antitumor effects in p53-deficient human colon tumor xenografts. Proc Natl Acad Sci U S A 2006; 103(29): 11003-8.
29. Wei Z, Zhou J, Yu H, *et al*. Zuo Jin Wan Reverses the Resistance of Colorectal Cancer to Oxaliplatin by Regulating the MALAT1/miR-200s/JNK Signaling Pathway. Evid Based Complement Alternat Med 2022; 2022: 3032407.
30. Lin F, Zhang G, Yang X, *et al*. A network pharmacology approach and experimental validation to investigate the anticancer mechanism and potential active targets of ethanol extract of Wei-Tong-Xin against colorectal cancer through induction of apoptosis via PI3K/AKT signaling pathway. J Ethnopharmacol 2023; 303: 115933.
31. Hu D, Meng RY, Nguyen TV, *et al*. Inhibition of colorectal cancer tumorigenesis by ursolic acid and doxorubicin is mediated by targeting the Akt signaling pathway and activating the Hippo signaling pathway. Mol Med Rep 2023; 27(1).
32. Sharma P, Shimura T, Banwait JK, *et al*. Andrographis-mediated chemosensitization through activation of ferroptosis and suppression of β-catenin/Wnt-signaling pathways in colorectal cancer. Carcinogenesis 2020; 41(10): 1385-1394.
33. Wang RR, Wang QQ, Jiang YL, *et al*. Advanced metastatic colorectal cancer treated with a combination of Jianpi Xiaoai Formula and chemotherapy. Chin J Tradit Chin Med Pharm 2016; 31(5): 5.
34. Yang X, Tang W, Jiang YL, *et al*. Effects of Jianpi Xiaoai Prescription on Cell Cycle and Apoptosis of Human Colon Cancer HCT116 Cells and Wnt/β-catenin Signaling Pathway Related Proteins. Chin J Informa Tradit Chin Med 2018; 25(6): 5.
35. Li WL. Clinical efficacy evaluation and study on anti-metastasis mechanism of jian hua tan prescription in colorectal metastases. Nanjing University of Chinese Medicine. 2020.
36. Liu XL and Chen SJ. Effect of the expression of si R NA targeting MMP-2 on the biological characteristics of colorectal cancer cells. J Bengbu Med College 2019; 44(10): 5.